

Identifying discontinuities of flood frequency curves

Arianna Miniussi^{1,2}, Ralf Merz^{1,3}, Lisa Kaule^{1,4}, Stefano Basso^{1,5}

¹Department of Catchment Hydrology, Helmholtz Centre for Environmental Research - UFZ, Halle
(Saale), Germany

²General Reinsurance, Cologne, Germany

³Institute of Geosciences and Geography, Martin-Luther University Halle-Wittenberg, Halle (Saale),
Germany

⁴Department of Hydrology, University of Bayreuth, Bayreuth, Germany

⁵Norwegian Institute for Water Research (NIVA), Oslo, Norway

Highlights:

- We develop an automated method to detect discontinuities of flood frequency curves
- We test it on observed and physically-based theoretical flood frequency curves
- We discuss the reliability of the physically-based approach to detect discontinuities

Corresponding author: Stefano Basso, stefano.basso@niva.no

14 **Abstract**

15 Discontinuities in flood frequency curves, here referred to as flood divides, hinder the esti-
16 mation of rare floods. In this paper we develop an automated methodology for the detection
17 of flood divides from observations and models, and apply it to a large set of case studies
18 in the USA and Germany. We then assess the reliability of the PHysically-based Extreme
19 Value (PHEV) distribution of river flows to identify catchments that might experience a
20 flood divide, validating its results against observations. This tool is suitable for the iden-
21 tification of flood divides, with a high correct detection rate especially in the autumn and
22 summer seasons. It instead tends to indicate the emergence of flood divides not visible
23 in the observations in spring and winter. We examine possible reasons of this behavior,
24 finding them in the typical streamflow dynamics of the concerned case studies. By means
25 of a controlled experiment we also re-evaluate detection capabilities of observations and
26 PHEV after discarding the highest maxima for all cases where both empirical and theoret-
27 ical estimates display flood divides. PHEV mostly confirms its capability to detect a flood
28 divide as observed in the original flood frequency curve, even if the shortened one does not
29 show it. These findings prove its reliability for the identification of flood divides and set the
30 premises for a deeper investigation of physiographic and hydroclimatic attributes controlling
31 the emergence of discontinuities in flood frequency curves.

32 **1 Introduction**

33 Despite considerable efforts to achieve reliable estimation of rare floods, these events are
34 still among the most common natural disasters (Wallemacq & House, 2018). The evaluation
35 of their hazard is however crucial for several applications, including the design of hydraulic
36 structures, risk planning and mitigation, and computation of premiums in the insurance
37 industry. Appraisal of the flood hazard is especially difficult when the magnitude of the
38 rarer floods can take values which are several times to orders of magnitude larger than
39 commonly observed floods, resulting in a marked uprise of the flood frequency curve beyond
40 certain return periods (Rogger et al., 2012; Smith et al., 2018).

41 Cognitive biases often lead to downplay the occurrence of such extreme events (B. Merz
42 et al., 2015, 2021), although the scientific literature repeatedly signalled the pervasiveness of
43 these behaviors terming them in various ways. In fact, heavy-tailed distributions of floods
44 (Farquharson et al., 1992; Bernardara et al., 2008; Villarini & Smith, 2010), inversions of

45 concavity and step changes in flood magnitude-frequency curves (Rogger et al., 2012; Guo
46 et al., 2014; Basso et al., 2016) and large values of the ratios between the maximum flood of
47 record and the sample flood with a specified recurrence time (Smith et al., 2018) and between
48 empirical high flow percentiles (Mushtaq et al., 2022) are all manifestations of a marked
49 increase of the magnitude of the rarer floods highlighted by means of different approaches.
50 To further stress the common nature of all these phenomena, in this study we favor none
51 of the previous locutions and instead label them as *flood divides*. The term was chosen to
52 highlight the existence of a discharge threshold which marks the rise of progressively larger
53 floods (red square in Figure 1d) and thus distinguishes between common and increasingly
54 extreme floods that may occur in river basins.

55 Rogger et al. (2012) investigated marked uprisings (i.e., discontinuities in the slope) of
56 flood frequency curves, which they called step changes, by leveraging information collected
57 from field surveys in two small alpine catchments to calibrate a distributed deterministic
58 rainfall-runoff model. They suggested that step changes occur when a threshold of the
59 catchment storage capacity is exceeded, and performed a synthetic experiment (Rogger et al.,
60 2013) to examine the effect of catchment storage thresholds and combined multiple controls
61 (e.g., the temporal variability of antecedent soil storage and the size of the saturated regions)
62 on the return period of the step change. They also highlighted important implications of the
63 presence or absence of flood divides for estimation and design purposes, further stressing the
64 need for a robust method to identify their possible occurrence. In fact, misidentifying the
65 presence of flood divides may either lead to overestimation of rare floods (if large recorded
66 outliers are considered in the analyses) or to their underestimation, in case events larger
67 than the flood divide were not yet recorded or are regarded as outliers.

68 Guo et al. (2014) and Basso et al. (2016) instead linked different shapes of flood fre-
69 quency curves and a marked growth of the magnitude of the rarer floods to the catchment
70 water balance. The former justified these features through the aridity index (i.e., the ra-
71 tio between mean annual potential evaporation and precipitation, Budyko (1974)), showing
72 that flood frequency curves characterized by increasing aridity index are steeper. The latter
73 explained them by means of the persistency index (i.e., the ratio between mean catchment
74 response time and runoff frequency, Botter et al. (2013)) and highlighted that the concavity
75 of the flood frequency curve changes from downward to upward shifting from persistent to
76 erratic regimes, thus causing the emergence of flood divides.

77 Smith et al. (2018) computed the ratio between the maximum flood of record and the
78 sample 10-year flood for thousands of gauges across the USA, finding large values for a
79 substantial amount of them. Different flood-generating processes (R. Merz & Blöschl, 2003;
80 Berghuijs et al., 2014; Tarasova et al., 2020) or mixtures of flood event types (Hirschboeck,
81 1987; Villarini & Smith, 2010; Smith et al., 2018) were indicated by other studies as possible
82 causes of these marked increases of the magnitude of the rarer floods.

83 Finally, a rather common approach to study this phenomenon consists in evaluating
84 the shape parameter of Generalized Extreme Value distributions fitted to observed annual
85 maximum series (Farquharson et al., 1992; Bernardara et al., 2008; Villarini & Smith,
86 2010; Smith et al., 2018). Notwithstanding the drawbacks of such a parametric approach
87 applied in association with limited records of annual maxima, these studies highlighted the
88 ubiquitous occurrence of flood divides and flood distributions characterized by thick upper
89 tails, as indicated by widespread positive values of the shape parameter. Moreover, Smith et
90 al. (2018) showed that the values of the shape parameter significantly increase with longer
91 data records. Their findings thus suggest that uprisings of flood frequency curves may be the
92 norm rather than rare conditions, pointing to the limited data record as the reason for the
93 latter belief.

94 Although former research hints at the ubiquitousness of flood divides in flood frequency
95 curves and provide indications of their possible drivers, a quantitative methodology to iden-
96 tify flood divides, which is robust to sampling uncertainty and tested in a large set of case
97 studies, is still lacking. The relevance of our study is thus twofold: (i) we develop such a
98 methodology for the detection of flood divides and evaluate their emergence across the US
99 and Germany, in a large set of catchments with contrasting physio-climatic features; (ii) we
100 examine the reliability of a process-based stochastic framework for the estimation of flood
101 frequency curves to detect flood divides and infer their occurrence, benchmarking its results
102 against observations.

2 Methodology and Data

2.1 The Physically-based Extreme Value distribution of river flows

2.1.1 Theoretical framework

The PHysically-based Extreme Value (PHEV) distribution of river flows is a parsimonious mechanistic-stochastic formulation of flood frequency curves (Basso et al., 2016, 2021) that stems from a rigorous mathematical description of catchment-scale daily soil moisture and streamflow dynamics in river basins (Laio et al., 2001; Porporato et al., 2004; Botter et al., 2007). In this framework, daily precipitation is represented as a marked-Poisson process with frequency $\lambda_P [T^{-1}]$ and exponentially-distributed depths with average value $\alpha [L]$. Soil moisture decreases due to evapotranspiration and is replenished by precipitation events that eventually trigger runoff pulses when an upper wetness threshold is crossed. These pulses, which feed water to a hydrologic storage, are also a Poisson process with frequency $\lambda < \lambda_P$ $[T^{-1}]$ and an exponential distribution of magnitudes with mean $\alpha [L]$. A non-linear (i.e., power-law) storage-discharge relation with parameters a and K epitomizes the hydrological response of the catchment and encompasses the joint effect of different flow components (Brutsaert & Nieber, 1977; Basso, Schirmer, & Botter, 2015).

The above-summarized mechanistic-stochastic description of runoff generation processes allows for expressing the probability distributions of daily flows (Botter et al., 2009) and peak flows (i.e., local flow peaks occurring as a result of streamflow-producing rainfall events) as a function of a few physically meaningful parameters (Basso et al., 2016). It also enables characterizing hydrologic regimes according to their typical streamflow dynamics, which are summarized by the persistency index (Botter et al., 2013). This is defined as the ratio between runoff frequency and the mean hydrograph recession rate, i.e., $\frac{\lambda}{K(\alpha\lambda)^{a-1}}$ (Basso et al., 2016; Deal et al., 2018).

An erratic regime (lower values of the persistency index), which is commonly found during dry seasons, very hot humid seasons with intense evapotranspiration or in fast responding catchments, is characterized by periods between the arrival of runoff-producing rainfall events which are longer than the typical duration of flow pulses. Conversely, a persistent regime (higher values of the persistency index), typically occurring in cold-humid seasons and lowland catchments, is characterized by frequent rainfall events and a rather constant water supply to the catchment.

134 Considering that peak flows in a given reference period (e.g., a season) are Poisson
 135 distributed and postulating their independence yield the probability distribution of flow
 136 maxima (i.e., maximum values in a specified timespan). The return period is finally obtained
 137 as the inverse of the exceedance cumulative probability of flow maxima, thus providing an
 138 expression of the flood frequency curve which reads (Basso et al., 2016):

$$T_r(q) = \frac{1}{1 - \exp[-\lambda\tau D_j(q)]} \quad (1)$$

139 where τ [T] is the duration in days of the reference period used in the analyses; $D_j(q) =$
 140 $\int_q^\infty p_j(q) dq$ is the exceedance cumulative probability of peak flows; p_j is the probability
 141 density function of peak flows, $p_j(q) = Cq^{1-a} \exp(\frac{\lambda q^{1-a}}{K(1-a)} - \frac{q^{2-a}}{\alpha K(2-a)})$; α and λ are the
 142 aforementioned parameters describing Poisson-distributed runoff events, a and K are the
 143 parameters of the power-law storage-discharge relation, and C is a normalization constant.

144 **2.1.2 Parameter Estimation**

145 The four parameters of PHEV (α , λ , a , K) are rather straightforward to estimate
 146 at the catchment scale. They are indeed directly derived from the observed time series
 147 of precipitation and streamflow: α is computed as the mean daily rainfall depth in rainy
 148 days, while λ (frequency of streamflow-producing rainfall) as the ratio between the long
 149 term mean daily flow $\langle q \rangle$ and α (Botter et al., 2007). The parameters of the power-law
 150 storage-discharge relation (i.e., the recession exponent a and coefficient K) are estimated
 151 through hydrograph recession analysis (Brutsaert & Nieber, 1977) following the approach
 152 proposed by Biswal and Marani (2010). Finally, the recession coefficient is not directly used
 153 as input in Eq. (1), but it is replaced by its maximum likelihood estimation on the observed
 154 seasonal flood frequency curve (Basso et al., 2016).

155 **2.2 Identification of Flood Divides**

156 To identify flood divides, we start from the method proposed by Rogger et al. (2013): a
 157 flood divide is defined as the sharpest bend of the flood frequency curve, here considered in
 158 terms of rescaled streamflow maxima (i.e., seasonal maxima divided by the long term mean
 159 daily flow, $\langle q \rangle$) as a function of the return period, the latter represented in logarithmic
 160 scale. We then develop a new methodology dedicated to its identification from both empirical
 161 estimates of the flood frequency curve obtained by means of Weibull plotting position and

162 models, such as PHEV. The resulting approach, which can be employed without depending
163 on subjective evaluation, is detailed in the following.

- 164 1. The curvature of the flood frequency curve, of which we show an example in Figure
165 1, is computed as $\log Tr'' / (1 + \log Tr'^2)^{(3/2)}$ (where the apex indicates the derivation
166 operation with respect to the rescaled streamflow) for both the observations and
167 PHEV. In the former case, we use the method developed by Jianchun et al. (1994)
168 for computing derivatives in non-equally spaced points, while for PHEV we employ
169 the Python routine from the Scipy library (*misc.derivative*), which uses a central
170 difference formula with spacing dx to compute the n^{th} derivative at a specified point.
- 171 2. As the noise associated to computing the curvature on a discrete and rather sparse
172 set of points (seasonal maxima) might lead to identification errors, a heuristic filter is
173 applied on the curvature calculated from observations: only points on the right-hand
174 side of the last value of the curvature exceeding the range $\pm\sigma$ (where σ indicates the
175 standard deviation of the curvature itself) are considered (Figure 1c);
- 176 3. The Mann-Whitney U-test (Mann & Whitney, 1947) is applied on the values of the
177 first derivatives on the left and right-hand sides of each potential flood divide identified
178 at point 2 to check if their distributions are statistically different at a significant level
179 equals to 0.05 (in other words, if the slope of the curve significantly differs between
180 the left and right-hand side of the flood divide); the effect size is then computed by
181 means of the Cohen's d (Cohen, 1974) to evaluate if the magnitude of the difference is
182 relevant (Sullivan & Feinn, 2012). For PHEV, this step is performed on a dense set of
183 values, equally spaced with an interval $\Delta q = 0.05$ up to a value of rescaled streamflow
184 equal to 200, i.e., 200 times the long-term average streamflow. The relative increment
185 of the slope between the left and right-hand side of a potential PHEV flood divide is
186 also evaluated within the observational range.
- 187 4. We finally identify as flood divide the point for which the p-value of the Mann-
188 Whitney test is the lowest, provided that the Cohen's d is greater than 0.4 (moderate
189 effect size; Gignac and Szodorai (2016); Lovakov and Agadullina (2021)) and the slope
190 increment exceeds a value of 1%.

191 Figure 1 visually exemplifies the application of the developed approach for flood divides
192 detection to the flood frequency curve of the Rott river at Kinning, Bavaria (ID: 18801005),
193 in the summer season. In Figure 1a the flood frequency curve is represented with switched

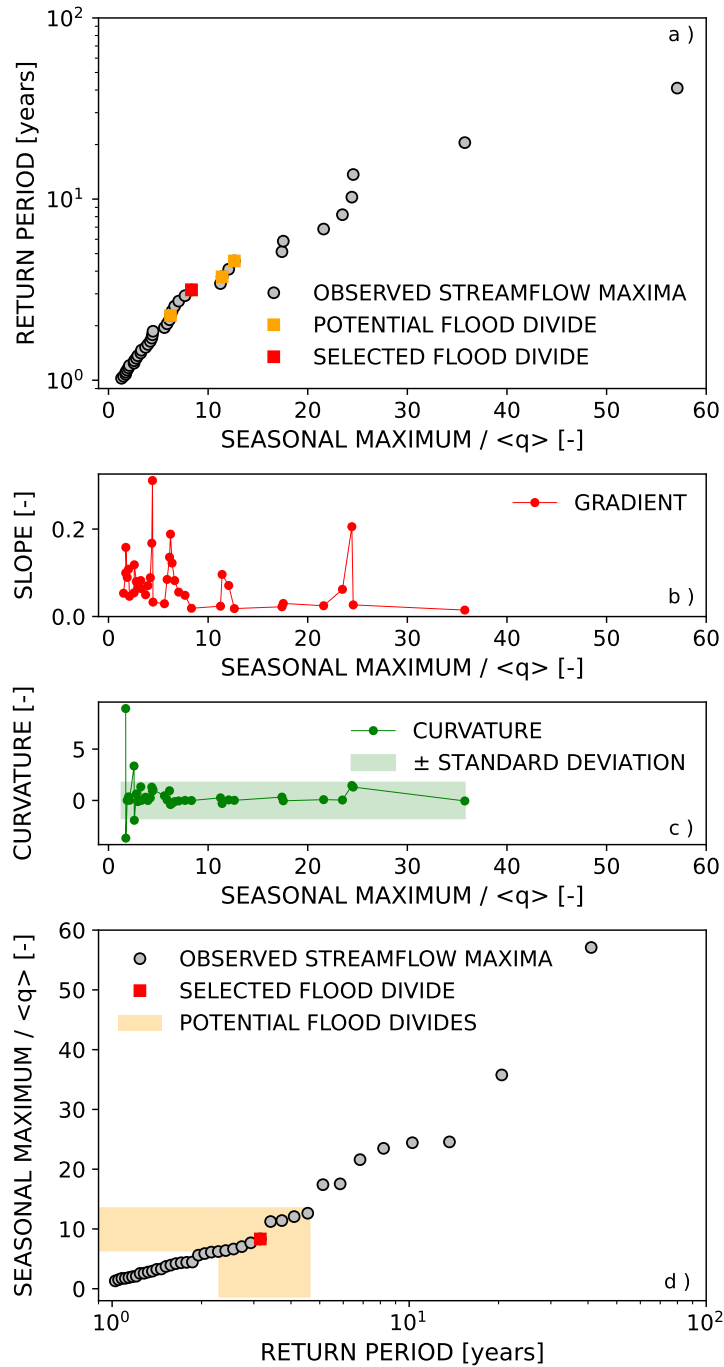


Figure 1: Exemplary application of the proposed methodology to detect flood divides to the Rott river at Kinning, Bavaria (ID: 18801005), in the summer season. a) Visualization of how the approach is actually applied, i.e., expressing the logarithm of the return period as a function of the rescaled seasonal maxima (gray filled circles). Potential flood divides (i.e., all the points with a p-value of the Mann-Whitney U-test lower than 0.05) are represented by orange squares, while the selected one (i.e., the one exhibiting the minimum p-value of the Mann-Whitney U-test and Cohen's d greater than 0.4) is depicted with a red square. b) First derivative computed on observations. c) Curvature computed on observations, with the shaded area representing twice its standard deviation. d) Standard representation of the flood frequency curve, namely observed maxima as a function of the logarithmic value of the return period (gray filled circles). The red square indicates the selected flood divide, while the orange shaded area represents the range of potential flood divides.

194 axes (i.e., the logarithm of the return period is represented on the y-axis whereas the rescaled
195 seasonal maxima on the x-axis), as streamflow is the independent variable in Eq. (1). The
196 red square in Figure 1a,d represents the selected flood divide, i.e., the one associated to
197 the lowest p-value of the Mann-Whitney U-test applied to the distributions of the first
198 derivatives (Figure 1b) and fulfilling the additional criterion on the Cohen's d . We also
199 show points that are initially analyzed as potential flood divides (i.e., all the points with a
200 Mann-Whitney p-value lower than 0.05, orange squares in Figure 1a).

201 **2.3 Datasets**

202 We use daily rainfall and streamflow time series from the Model Parameter Estimation
203 Experiment dataset (MOPEX, data from 1948 to 2003) (Duan et al., 2005; Schaake et
204 al., 2006) and from Germany (1951-2013) (Tarasova et al., 2018). Streamflow is measured
205 at the gauging stations whose geographical coordinates are listed in Table S1, whereas
206 the corresponding rainfall records are spatially averaged values for the upstream drainage
207 areas derived from gridded datasets. We perform all analyses in a seasonal time frame
208 (spring: March to May; summer: June to August; autumn: September to November; winter:
209 December to February) to account for the seasonality of rainfall and runoff (Allamano et
210 al., 2011; Baratti et al., 2012). To assure that PHEV suitably represents the key processes
211 of streamflow generation in the set of case studies, we only consider catchments with low
212 human impact, weak or absent inter-seasonal snow dynamics (Botter et al., 2013; Wang
213 & Hejazi, 2011) and hydrograph recession properties which are independent of the peak
214 flow (Basso et al., 2021). Similarly to previous studies (R. Merz et al., 2020), we as well
215 restrict our analysis to cases for which the root mean square error ($RMSE$) between the
216 predicted and observed flood frequency curve is limited (i.e., lower than 0.3), as a fairly
217 accurate estimation of the flood frequency curve is a precondition to investigate if PHEV is
218 able to correctly identify flood divides and whether their occurrence is affected by physio-
219 climatic catchment attributes. Figure S1 provides a summary of the performance of PHEV
220 (quantified by means of varied error metrics, see Supplementary Material) in reproducing
221 observed flood frequency curves in the considered set of case studies. This selection yields a
222 set of 101 case studies (i.e., catchment-season combinations), divided into 23, 29, 23 and 26
223 cases respectively in the spring, summer, autumn and winter seasons. The median length
224 of the considered data series is 54 years (min: 34, max: 55) for the MOPEX and 58 years

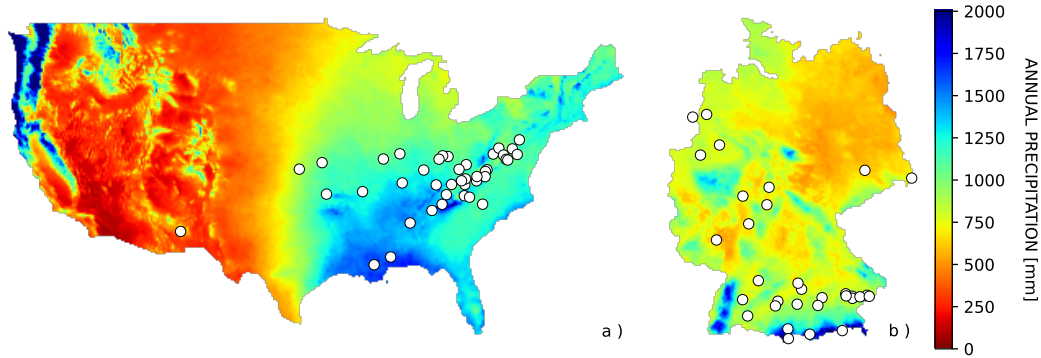


Figure 2: Select river basins (white filled circles) from the (A) MOPEX and (B) German datasets. The background of the maps represents 30-years annual precipitation normals (1981-2010 for the US and 1991-2020 for Germany).

225 (min: 40, max: 63) for the German case studies. Their catchment areas vary between 43
 226 and 9052 km² (median: 865 km²). The locations of their outlets are displayed in Figure 2.

227 3 Results and Discussion

228 We apply the methodology for the identification of flood divides introduced in the
 229 previous section to each observed and analytic seasonal flood frequency curve, thus allowing
 230 for evaluating the flood divide detection of PHEV against observations, which we consider
 231 as benchmark (Figure 3). The bar plots in Figure 3 show the percentages of case studies
 232 for which a flood divide is identified from both PHEV and the observational records (true
 233 positives, dark green color), those which display a flood divide neither in the empirical nor
 234 in the analytic flood frequency curves (true negatives, light green), the percentages of cases
 235 where a flood divide is detected from the observations but not from the analytical model
 236 (false negatives, red), and those where the analytical model has foreseen the occurrence of
 237 a flood divide which is not confirmed by the available observations (false positives, orange).
 238 The existence of both true positives and true negatives emphasizes the capability of PHEV
 239 to mimic varied observed shapes of flood frequency curves (Basso et al., 2016) and to identify
 240 both the presence and the absence of a flood divide.

241 The bar plots in Figure 3a and 3b differ for the criteria applied in the flood divide iden-
 242 tification methodology. In Figure 3a only the controls on the p-value of the Mann-Whitney
 243 U-test mentioned in Section 2.2 are considered, whereas the additional requirements on the
 244 effect size and slope increment are as well used in Figure 3b. True positives (dark green)

245 prevail in the summer (18 cases) and autumn (14 cases) seasons of Figure 3a, amounting
246 to about 60% of the cases. False positives constitute instead a sizable share of the cases in
247 spring (12 cases) and winter (21 cases). When more stringent requirements for the identi-
248 fication of flood divides are used, by accounting for the mentioned additional criteria, the
249 percentage of true positives decreases (Figure 3b, dark green; respectively 3, 11, 12 and 1
250 cases in spring, summer, autumn and winter). A few cases of those shifting category be-
251 come true negatives (for an overall number of 2, 3, 1 and 1 cases in spring, summer, autumn
252 and winter), indicating that the slope of the flood frequency curve does not substantially
253 increases on the right-hand side of the potential flood divide, thus not representing a note-
254 worthy hazard. Most of them however become false positives (orange color in Figure 3b;
255 respectively 18, 15, 9 and 24 cases in spring, summer, autumn and winter) as the identified
256 changes of the slope of the observed flood frequency curve are not substantial according to
257 the limited amount of available observations, whereas PHEV confirms the existence of a
258 flood divide thanks to its evaluation in an unlimited number of points. Consistent results
259 are also found when considering different significant levels for the Mann-Whitney test: the
260 strictest the level the highest the share of cases shifting between true and false positives,
261 which once again points to the unfeasibility of detecting flood divides with confidence from
262 plain observations.

263 The predominance of false positives in spring (18 cases) and winter (24 cases) (orange
264 color in Figure 3b) calls for further investigation of their causes. We therefore hypothesize
265 that PHEV, by leveraging the embedded mechanistic description of hydro-climatic dynamics
266 taking place in watersheds and the information gained from analyzing daily rainfall and
267 streamflow series, might indicate the possible emergence of flood divides that are not yet
268 displayed by the observed flood frequency curves. In fact, these empirical estimates are
269 likely affected by small sizes of the samples of large events (i.e., those on the right-hand side
270 of each potential flood divide, see Figure 1a) and by the specific character of catchments,
271 which may have a more or less enhanced propensity to exhibit extreme floods and thus
272 display them in a limited data record. We then perform the following experiment to test
273 this hypothesis. We consider the set of true positives (i.e., the 27 cases for which both
274 PHEV as well as the observed flood frequency curve show a flood divide) and retain only
275 maxima with return periods below 5 years (see an explanatory example in Figure 4a, where
276 the maxima retained are represented by gray filled circles with blue contours). In so doing,
277 we approximately discard in each case the largest ten points and their corresponding years

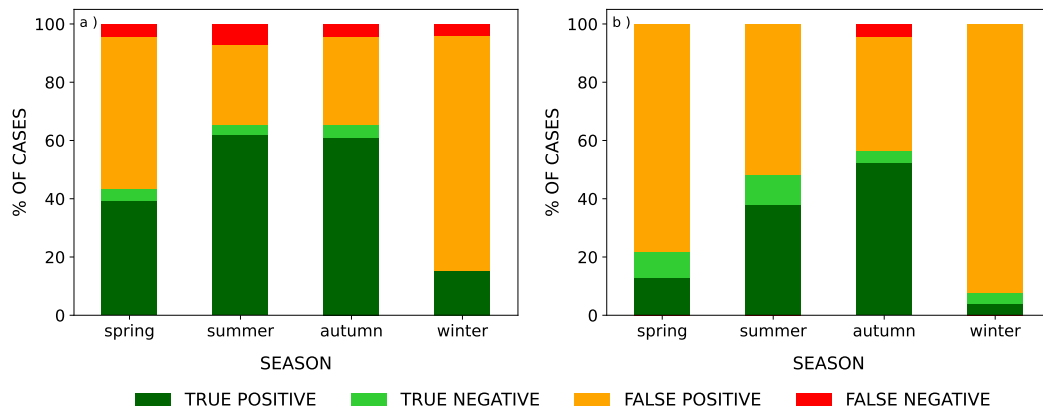


Figure 3: Performance of the PHysically-based Extreme Value (PHEV) distribution of river flows in the detection of flood divides when only the controls on the Mann-Whitney U-test are considered (see Section 2.2, panel a) and when the whole methodology for detecting flood divides is applied (see Section 2.2, panel b). Percentages are calculated on the overall number of case studies, which amount to 23, 29, 23 and 26 cases respectively in the spring, summer, autumn and winter seasons. True positives (dark green color; 27 cases in panel b) and true negatives (light green; 7 cases) indicate coherence between PHEV and observations, i.e., flood divides are either detected or not from both PHEV and the observed records. These constitute a large number of cases in summer (14 cases) and autumn (13 cases). False positives (orange; 66 cases) and false negatives (red; 1 case) represent the cases in which either PHEV detects a flood divide that was not identified by the observations or the observations display a flood divide which is not detected by PHEV. The indicated absolute numbers of positive and negative cases refer to the complete application of the methodology for detecting flood divides (i.e., panel b). The reasons for the presence of false positives are further investigated in the study and clarified in the text and figures.

278 of occurrence. Thereby, fictitious flood frequency curves only comprising maxima with
279 smaller magnitudes (and return periods) are created, thus reproducing the conditions we
280 hypothesized as possible reasons of the emergence of false positives. We then apply the
281 usual methodology for identifying flood divides on these fictitious flood frequency curves
282 and the corresponding shortened data records.

283 PHEV detects a true flood divide (i.e., true positives) in 81% of the cases (22 case
284 studies) even when the largest points are removed, whereas the observations only in 40%
285 (11 cases). The maps in Figure 4b and 4c summarize this result: half circles are colored
286 either in green, if a flood divide is successfully detected from the shortened flood frequency
287 curve, or in red in the opposite case. The left half of the circle depicts the detection
288 capability of PHEV, while the right side the results obtained from the observations. It can
289 be easily seen that most left halves of the circles are colored in green and most of the right
290 ones are instead red, thus indicating a high success rate of PHEV and a significantly lower
291 one of observations in inferring the emergence of flood divides from shortened records. A
292 similar result is obtained by discarding maxima with return period greater than 10 years
293 (i.e., discarding about five-six points instead of the highest ten), when PHEV correctly
294 detects 85% of true flood divides (23 cases) in comparison to a correct detection rate from
295 observations of 60% (16 cases). The outcome of this experiment strongly suggests that the
296 detected false positives (orange color in Figure 3) indeed arise because of the statistical
297 uncertainty of limited data records and the capability of PHEV to infer the occurrence of
298 flood divides from short series rather than by its inability to correctly identify inflection
299 points which were detected (or not) in the observed flood frequency curves.

300 A physical explanation of the reason why some observational series might not exhibit a
301 flood divide which shall be expected is provided by considering typical streamflow dynamics
302 occurring for distinct river flow regimes, here characterized by means of the persistency
303 index (Botter et al., 2013). When streamflow values weakly oscillate around their mean
304 (persistent regimes), the probability of occurrence of relatively large flows is very low, and
305 extreme events are unlikely to be captured by short time series. On the contrary, erratic
306 regimes are composed of a sequence of high flows interspersed in between prolonged periods
307 of low flows. Events which are several times (i.e., order of magnitudes) higher than the
308 average flow are thus more likely to occur in these regimes (Basso, Frascati, et al., 2015). In
309 the context of this study, false positives shall therefore mostly occur for persistent regimes,

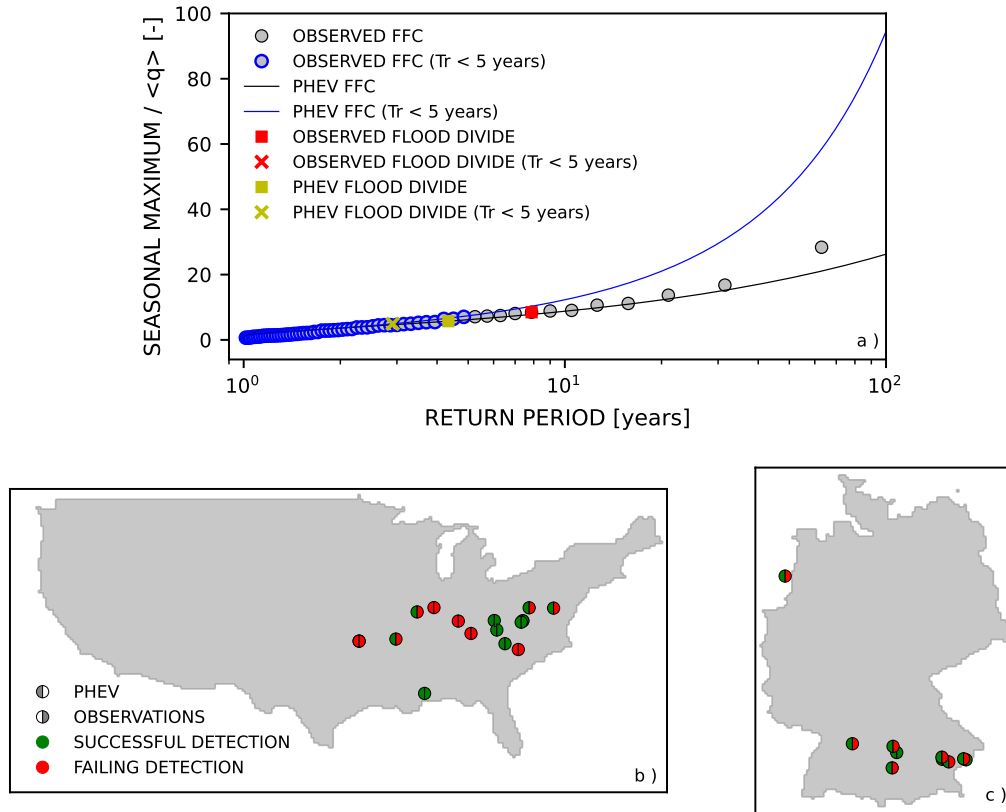


Figure 4: Visual explanation and results of an experiment aimed at testing hypotheses on the emergence of false positives. a) Gray dots with black (blue) contour represent the complete (shortened, until a return period of 5 years) observed seasonal maxima series of the Wörnitz river at Harburg, Bayern (ID:11809009), in the summer season. The solid black (blue) line displays the analytic flood frequency curve (i.e., PHEV) whose parameters are estimated from the complete (shortened) time series. The red (yellow) square indicates the flood divide detected from the observations (by PHEV) using the complete series, while the corresponding crosses (the red one is not visible in the plot as no flood divide was detected after shortening the observations) represent the observed and analytic flood divides detected on the shortened flood frequency curve. b-c) Locations of the true positives in the US (panel b) and Germany (panel c). The left (right) half of the circles represent PHEV (observations) ability to detect a flood divide when the shortened flood frequency curves (i.e., maxima characterized by return period below 5 years) are used. The green (red) colored halves indicate successful (failing) detection. Remarkably, most of the left halves are green (PHEV detects true flood divides even from the shortened series in the majority of the cases), whereas most of the right ones are red (flood divides are not always identified from observations when the shortened records are used).

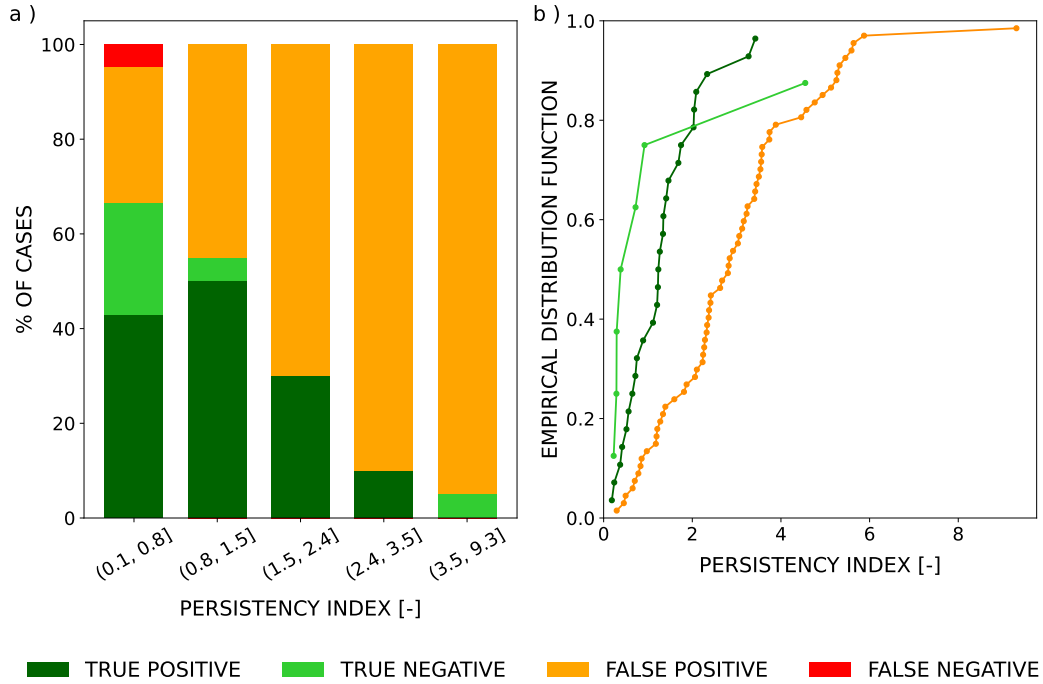


Figure 5: a) Performance of the PHysically-based Extreme Value (PHEV) distribution of river flows in the detection of flood divides as a function of the persistency index. Ranges (whose boundaries are reported in the x-axis) were set so as to have an equal number of values (~ 20) per bin. b) Empirical cumulative distribution functions of the persistency index for true positive (dark green), true negative (light green) and false positive (orange) cases. The distributions of true versus false cases are significantly different in a statistical sense (the p-value of the 2-samples Kolmogorov-Smirnov test is lower than 0.01.)

310 as such large events enabling detection of flood divides from empirical flood frequency curves
 311 are less likely to have been observed during the available data record.

312 Figure 5a displays the percentages of true positives (dark green color; from left to
 313 right: 9, 10, 6, 2 and 0 cases), true negatives (light green; respectively 5, 1, 0, 0, 1 cases),
 314 false negatives (red; 1, 0, 0, 0, 0 cases) and false positives (orange; from left to right: 6,
 315 9, 14, 18 and 19 cases) for five ranges of the persistency index set so as to have an equal
 316 number of values (~ 20) per bin. The number of false positives consistently increases with
 317 the persistency index, thus corroborating the above reasoning. No clear patterns are instead
 318 observed with, e.g., the drainage area and the average rainfall magnitude in the catchment
 319 (Figure S3), which are sometimes regarded as possible drivers of a marked increase of the
 320 magnitude of the rarer floods (Gaume, 2006; Villarini & Smith, 2010).

321 A recent review of the current scientific knowledge (B. Merz et al., 2022) suggests
 322 explanations for these results. It signals an unlikely direct role of catchment size in deter-

323 mining tail behaviors of flood distributions, as increasing drainage areas entail both spatial
324 aggregation (which may cause lighter tails), and shifts of dominant processes (e.g., different
325 precipitation types and runoff generation mechanisms) which may lead in the opposite di-
326 rection. It also reports robust evidences against a dominant role of rainfall characteristics
327 for the emergence of heavy-tailed flood distributions, as runoff generation processes strongly
328 modulate the hydrologic response. On the contrary, the available literature emphasizes the
329 role of non-linear hydrological responses and the catchment water balance for the emergence
330 of heavy tails. These are the two key processes described by PHEV and summarized by the
331 persistency index, which thus arises as a pivotal indicator of the possibility to detect flood
332 divides from data records.

333 To further highlight the relation between typical river flow dynamics recapped in the
334 persistency index and the occurrence of false positives we compare in Figure 5b the cumula-
335 tive distributions of the persistency index for true cases (green) and false positives (orange).
336 The distributions clearly differ. True cases feature more erratic regimes which facilitate their
337 identification from data records, whereas false positives mostly occur for persistent regimes.
338 This qualitative evaluation is validated by applying the 2-sample Kolmogorov-Smirnov test,
339 which evaluates if two samples come from the same distribution (null-hypothesis), to the
340 sets of true and false positives (the same is obtained by comparing true negatives and false
341 positives). We can reject the null-hypothesis at the 0.01 significance level, meaning that
342 the two samples are drawn from different distributions and false positives are significantly
343 more likely to occur for persistent regimes. The same cannot be proved for the cumulative
344 distributions of catchment area (p-value = 0.44) and average rainfall magnitude (p-value =
345 0.34) for the sets of true and false positives. Remarkably, the seasons characterized by the
346 larger portion of false positives are spring and winter, during which regimes tend to be more
347 persistent.

348 The physical explanation provided here of the different telling power of streamflow data
349 for rivers characterized by distinctively different streamflow dynamics agrees with the results
350 of previous research. For example, Botter et al. (2013) showed less variable streamflow
351 distributions across years in erratic regimes compared to persistent ones, which determines
352 higher representativeness of their estimates in the former case for a given length of the data
353 record. Smith et al. (2018) also demonstrated that upper tail ratios grow with the length
354 of data and, for a given data length, are larger (i.e., flood divides are more often identified)
355 in arid and semiarid regions than in humid ones. Their results jointly suggest that, given

356 similarly long data records, the typical (erratic) flow dynamics of drier areas enable more
357 reliable characterization of the whole range of values possibly spanned by streamflow and
358 of the presence or absence of flood divides according to the physical explanation provided
359 above.

360 **4 Concluding Remarks**

361 In this work we examine the occurrence of marked uprisings of flood frequency curves
362 (termed flood divides), which are pivotal for a correct estimation of river flood hazard. We
363 develop a robust methodology to identify them from observational records and models, and
364 evaluate the capability of the PHysically-based Extreme Value distribution of river flows
365 (PHEV) to reliably detect flood divides.

366 Results show that PHEV is consistently able to recognize the presence/absence of flood
367 divides in a large set of case studies from the US and Germany. Possible reasons for the
368 occurrence of a sizeable number of false positives are investigated by accounting for both
369 the statistical uncertainty of relatively short observational records and the typical hydro-
370 climatic variability of different river basins, which affects the information content of these
371 limited data series. To this end, we perform a controlled experiment in which we remove
372 the highest flow maxima in the flood frequency curves of the true positive cases and repeat
373 the flood divide detection analysis on the shorter series, showing that PHEV can foresee
374 the emergence of true flood divides in more than 80% of the cases even if the shortened
375 observations do not display them. The result supports claims of the dependability of flood
376 divides initially classified as false positives. An investigation of the intrinsic dynamics of
377 streamflows in the set of true and false positives further elucidates the issue. False positives
378 are indeed preferentially found for more persistent regimes (87% of the false positives have
379 persistency index above two, as opposed to only 11% of true positives; the overall number
380 of cases with persistency index above two is 55) which, by their nature, rarely exhibit large
381 extreme flow values. The limited length of the available observed time series might be thus
382 constraining the possibility to observe expected flood divides, analogously to what occurs
383 when we artificially reduce the size of the observational sample.

384 The present analysis, performed on a wide set of catchments characterized by different
385 hydroclimatic features, reveals PHEV as a reliable tool to identify and foresee the occurrence
386 of flood divides and consequently unveil the propensity of rivers to large floods. The method

387 is especially relevant in data scarce conditions, although limitations linked to the domain
388 of applicability of this tools exist and have been recalled in this work. The study lays
389 the foundations for a better comprehension of climate and landscape controls of observed
390 marked rises of the magnitude of the rarer floods, which is the subject of ongoing research.

391 **Acknowledgments**

392 This work is funded by the Deutsche Forschungsgemeinschaft (DFG, German Research
393 Foundation) - Project Number 421396820 'Propensity of rivers to extreme floods: climate-
394 landscape controls and early detection (PREDICTED)' and Research Group FOR 2416
395 'Space-Time Dynamics of Extreme Floods (SPATE)'. The financial support of the Helmholtz
396 Centre for Environmental Research - UFZ is as well acknowledged. We thank the Bavar-
397 ian State Office of Environment (LfU, <https://www.gkd.bayern.de/de/fluesse/abfluss>)
398 and the Global Runoff Data Centre (GRDC) prepared by the Federal Institute for Hy-
399 drology (BfG, <http://www.bafg.de/GRDC>) for providing the discharge data for Germany.
400 The MOPEX dataset is available at [https://hydrology.nws.noaa.gov/pub/gcip/mopex/
401 US_Data/](https://hydrology.nws.noaa.gov/pub/gcip/mopex/US_Data/). 30-year normal precipitation gridded data for the US are provided by the PRISM
402 Climate Group, Oregon State University, <http://prism.oregonstate.edu> (downloaded on
403 June, 1st 2021); 30-year normal precipitation gridded data for Germany are provided by
404 the Deutsche Wetter Dienst (DWD) at [https://opendata.dwd.de/climate_environment/
405 CDC/grids_germany/multi-annual/precipitation/](https://opendata.dwd.de/climate_environment/CDC/grids_germany/multi-annual/precipitation/)

406 **References**

- 407 Allamano, P., Laio, F., & Claps, P. (2011). Effects of disregarding seasonality on the
408 distribution of hydrological extremes. *Hydrol. Earth Syst. Sci.*, *15*, 3207–3215. doi:
409 doi:10.5194/hess-15-3207-2011
- 410 Baratti, E., Montanari, A., Castellarin, A., Salinas, J. L., Viglione, A., & Bezzi, A. (2012).
411 Estimating the flood frequency distribution at seasonal and annual time scales. *Hydrol.*
412 *Earth Syst. Sci.*, *16*, 4651-4660. doi: 10.5194/hess-16-4651-2012
- 413 Basso, S., Botter, G., Merz, R., & Miniussi, A. (2021). Phev! the physically-based extreme
414 value distribution of river flows. *Environ. Res. Lett.*, *16*, 124065. doi: 10.1088/
415 1748-9326/ac3d59
- 416 Basso, S., Frascati, A., Marani, M., Schirmer, M., & Botter, G. (2015). Climatic and
417 landscape controls on effective discharge. *Geophysical Research Letters*, *42*, 8441–8447.

418 doi: 10.1002/2015GL066014

419 Basso, S., Schirmer, M., & Botter, G. (2015). On the emergence of heavy-tailed streamflow
420 distributions. *Advances in Water Resources*, *82*, 98 - 105. doi: 10.1016/j.advwatres
421 .2015.04.013

422 Basso, S., Schirmer, M., & Botter, G. (2016). A physically based analytical model of flood
423 frequency curves. *Geophysical Research Letters*, *43*(17), 9070-9076. doi: 10.1002/
424 2016GL069915

425 Berghuijs, W. R., Sivapalan, M., Woods, R. A., & Savenije, H. (2014). Patterns of similarity
426 of seasonal water balances: A window into streamflow variability over a range of time
427 scales. *Water Resources Research*, *50*, 5638 - 5661. doi: 10.1002/2014WR015692

428 Bernardara, P., Schertzer, D., Eric, S., Tchiguirinskaia, I., & Lang, M. (2008). The flood
429 probability distribution tail: How heavy is it? *Stochastic Environmental Research and
430 Risk Assessment*, *22*, 5638 - 5661. doi: 10.1002/2014WR015692

431 Biswal, B., & Marani, M. (2010). Geomorphological origin of recession curves. *Geophysical
432 Research Letters*, *37*(24). (L24403) doi: 10.1029/2010GL045415

433 Botter, G., Basso, S., Rodriguez-Iturbe, I., & Rinaldo, A. (2013). Resilience of river flow
434 regimes. *Proceedings of the National Academy of Sciences*, *110*(32), 12925-12930. doi:
435 10.1073/pnas.1311920110

436 Botter, G., Porporato, A., Rodriguez-Iturbe, I., & Rinaldo, A. (2007). Basin-scale soil mois-
437 ture dynamics and the probabilistic characterization of carrier hydrologic flows: Slow,
438 leaching-prone components of the hydrologic response. *Water Resources Research*,
439 *43*(2). doi: 10.1029/2006WR005043

440 Botter, G., Porporato, A., Rodriguez-Iturbe, I., & Rinaldo, A. (2009). Nonlinear storage-
441 discharge relations and catchment streamflow regimes. *Water Resources Research*,
442 *45*(10). doi: 10.1029/2008WR007658

443 Brutsaert, W., & Nieber, J. L. (1977, 6). Regionalized drought flow hydrographs from a
444 mature glaciated plateau. *Water Resources Research*, *13*(3), 637-643. doi: 10.1029/
445 WR013i003p00637

446 Budyko, M. (1974). *Climate and life*. Academic Press.

447 Cohen, J. (1974). *Statistical power analysis for the behavioral sciences*. Lawrence Erlbaum
448 Associates.

449 Deal, E., Braun, J., & Botter, G. (2018). Understanding the role of rainfall and hydrology in
450 determining fluvial erosion efficiency. *Journal of Geophysical Research: Earth Surface*,

451 123(4), 744-778. doi: 10.1002/2017JF004393

452 Duan, Q., Shaake, J., Andreassian, V., S., F., Goteti, G., Gupta, H., ... Wood, E. (2005).
453 Model parameter estimation experiment (mopex): An overview of science strategy
454 and major results from the second and third workshops. *Journal of Hydrology*, 320,
455 3 - 17. doi: 10.1016/j.jhydrol.2005.07.031

456 Farquharson, F. A. K., Meigh, J. R., & Sutcliffe, J. (1992). Regional flood frequency
457 analysis in arid and semi-arid areas. *J. Hydrol.*, 138(3), 487-501. doi: 10.1016/
458 0022-1694(92)90132-F

459 Gaume, E. (2006). On the asymptotic behavior of flood peak distributions. *Hydrol. Earth*
460 *Syst. Sci.*, 10, 233-243.

461 Gignac, G. E., & Szodorai, E. T. (2016). Effect size guidelines for individual differences
462 researchers. *Personality and Individual Differences*, 102, 74-78. doi: 10.1016/j.paid
463 .2016.06.069

464 Guo, J., Li, H.-Y., Leung, L. R., Guo, S., Liu, P., & Sivapalan, M. (2014). Links be-
465 tween flood frequency and annual water balance behaviors: A basis for similarity and
466 regionalization. *Water Resources Research*, 50. doi: 10.1002/2013WR014374

467 Hirschboeck, K. (1987). Hydroclimatically-defined mixed distributions in partial dura-
468 tion flood series. In *In: Singh v.p. (eds) hydrologic frequency modeling* (p. 199-
469 212). Louisiana State University, Baton Rouge, U.S.A: Springer, Dordrecht. doi:
470 10.1007/978-94-009-3953-0_13

471 Jianchun, L., Pope, G. A., & Sepehrnoori, K. (1994). A high-resolution finite-difference
472 scheme for nonuniform grids. *Appl. Math. Modelling*, 19, 162 - 172.

473 Laio, F., Porporato, A., Ridolfi, L., & Rodriguez-Iturbe, I. (2001). Plants in water-controlled
474 ecosystems: active role in hydrologic processes and response to water stress: Ii. prob-
475 abilistic soil moisture dynamics. *Advances in Water Resources*, 24(7), 707 - 723. doi:
476 10.1016/S0309-1708(01)00005-7

477 Lovakov, A., & Agadullina, E. R. (2021). Empirically derived guidelines for effect size
478 interpretation in social psychology. *European Journal of Social Psychology*, 51(3),
479 485-504. doi: 10.1002/ejsp.2752

480 Mann, H. B., & Whitney, D. R. (1947). On a Test of Whether one of Two Random Variables
481 is Stochastically Larger than the Other. *The Annals of Mathematical Statistics*, 18(1),
482 50 - 60. doi: 10.1214/aoms/1177730491

483 Merz, B., Basso, S., Fischer, S., Lun, D., Blöschl, G., Merz, R., ... Schumann, A. (2022).

484 Understanding heavy tails of flood peak distributions. *Water Resources Research*,
485 58(6), e2021WR030506. doi: 10.1029/2021WR030506

486 Merz, B., Blöschl, G., Vorogushyn, S., & et al. (2021). Causes, impacts and patterns
487 of disastrous river floods. *Nat. Rev. Earth Environ.*, 2, 592 – 609. doi: 10.1038/
488 s43017-021-00195-3

489 Merz, B., Vorogushyn, S., Lall, U., Viglione, A., & Blöschl, G. (2015). Charting unknown
490 waters — on the role of surprise in flood risk assessment and management. *Water*
491 *Resources Research*, 51, 6399 – 6416. doi: 10.1002/2015WR017464

492 Merz, R., & Blöschl, G. (2003). A process typology of regional floods. *Water Resources*
493 *Research*, 39, 9578 – 9591. doi: 10.1029/2002WR001952

494 Merz, R., Tarasova, L., & Basso, S. (2020). Parameter’s controls of distributed catchment
495 models—how much information is in conventional catchment descriptors? *Water*
496 *Resources Research*, 56(2), e2019WR026008. doi: 10.1029/2019WR026008

497 Mushtaq, S., Miniussi, A., Merz, R., & Basso, S. (2022). Reliable estimation of high
498 floods: A method to select the most suitable ordinary distribution in the metasta-
499 tistical extreme value framework. *Advances in Water Resources*, 161, 104127. doi:
500 10.1016/j.advwatres.2022.104127

501 Porporato, A., Daly, E., & Rodriguez-Iturbe, I. (2004). Soil water balance and ecosystem
502 response to climate change. *The American Naturalist*, 164, 625–632. doi: 10.1086/
503 424970

504 Rogger, M., Pirkl, H., Viglione, A., Komma, J., Kohl, B., Kirnbauer, R., ... Blöschl, G.
505 (2012). Step changes in the flood frequency curve: process controls. *Water Resources*
506 *Research*, 48, W05544. doi: 10.1029/2011WR011187

507 Rogger, M., Viglione, A., Derx, J., & Blöschl, G. (2013). Quantifying effects of catchments
508 storage thresholds on step changes in the flood frequency curve. *Water Resources*
509 *Research*, 49, 6946–6958. doi: 10.1002/wrcr.20553

510 Schaake, J., Duan, Q., Andréassian, V., Franks, S., Hall, A., & Leavesley, G. (2006). The
511 model parameter estimation experiment (mopex). *Journal of Hydrology*, 320(1), 1 -
512 2. (The model parameter estimation experiment) doi: 10.1016/j.jhydrol.2005.07.054

513 Smith, J. A., Cox, A. A., Baeck, M. L., Yang, L., & Bates, P. D. (2018). Strange floods:
514 The upper tail of flood peaks in the united states. *Water Resources Research*, 54,
515 6510-6542. doi: 10.1029/2018WR022539

516 Sullivan, G., & Feinn, R. (2012). Using effect size — or why the p value is not enough.

- 517 *Journal of Graduate Medical Education*, 279-282. doi: 10.4300/JGME-D-12-00156.1
- 518 Tarasova, L., Basso, S., & Merz, R. (2020). Transformation of generation processes
519 from small runoff events to large floods. *Geophysical Research Letters*, 47(22),
520 e2020GL090547. doi: 10.1029/2020GL090547
- 521 Tarasova, L., Basso, S., Zink, M., & Merz, R. (2018). Exploring controls on rainfall-runoff
522 events: 1. Time series-based event separation and temporal dynamics of event runoff
523 response in Germany. *Water Resources Research*, 54, 7711 - 7732. doi: 10.1029/
524 2018WR022587
- 525 Villarini, G., & Smith, J. (2010). Flood peak distributions for the eastern united states.
526 *Water Resources Research*, 46. doi: 10.1029/2009WR008395
- 527 Wallemacq, P., & House, R. (2018). *Economic Losses, Poverty & Disasters 1998-2017* (Tech.
528 Rep.). United Nations Office for Disaster Risk Reduction (UNDRR) and Centre for
529 Research on the Epidemiology of Disasters (CRED).
- 530 Wang, D., & Hejazi, M. (2011). Quantifying the relative contribution of the climate and
531 direct human impacts on mean annual streamflow in the contiguous United States.
532 *Water Resources Research*, 47. doi: 10.1029/2010WR010283